

This article was downloaded by: [University North Carolina - Chapel Hill]

On: 14 November 2011, At: 18:08

Publisher: Taylor & Francis

Informa Ltd Registered in England and Wales Registered Number: 1072954 Registered office: Mortimer House, 37-41 Mortimer Street, London W1T 3JH, UK



Philosophical Magazine A

Publication details, including instructions for authors and subscription information:

<http://www.tandfonline.com/loi/tpha20>

An HREM study of the defects in ZnS

L. C. Qin^a, D. X. Li^a & K. H. Kuo^a

^a Institute of Metal Research, Academia Sinica, 110015, Shenyang, P.R. China

Available online: 26 Oct 2009

To cite this article: L. C. Qin, D. X. Li & K. H. Kuo (1986): An HREM study of the defects in ZnS, Philosophical Magazine A, 53:4, 543-555

To link to this article: <http://dx.doi.org/10.1080/01418618608242852>

PLEASE SCROLL DOWN FOR ARTICLE

Full terms and conditions of use: <http://www.tandfonline.com/page/terms-and-conditions>

This article may be used for research, teaching, and private study purposes. Any substantial or systematic reproduction, redistribution, reselling, loan, sub-licensing, systematic supply, or distribution in any form to anyone is expressly forbidden.

The publisher does not give any warranty express or implied or make any representation that the contents will be complete or accurate or up to date. The accuracy of any instructions, formulae, and drug doses should be independently verified with primary sources. The publisher shall not be liable for any loss, actions, claims, proceedings, demand, or costs or damages whatsoever or howsoever caused arising directly or indirectly in connection with or arising out of the use of this material.

An HREM study of the defects in ZnS

By L. C. QIN, D. X. LI and K. H. KUO

Institute of Metal Research, Academia Sinica, 110015 Shenyang, P.R. China

[Received 26 April 1985 and accepted 29 August 1985]

ABSTRACT

High-resolution electron microscopy (HREM) has been used to investigate the defect structures in ZnS crystals of zincblende type with $\langle 110 \rangle$ beam incidence. It is concluded that there is a high density of 180° rotation twins. Under different imaging conditions the bright dots in the HREM micrographs may either correspond to the atomic column pairs or the structural channels surrounded by atoms, and these make the twin boundary appear in different forms by changing experimental parameters. End-on extended dislocations which are formed by the dissociation of 60° mixed dislocation and 0° screw dislocation with Burgers vectors of $\frac{1}{2}\langle 110 \rangle$ type were analysed and characterized. Using anisotropic elasticity theory of dislocations and the width of dissociation measured from HREM images, the stacking fault energy on the $\{111\}$ plane in ZnS has been determined to be $2.7 \pm 0.1 \text{ mJm}^{-2}$. Frank dislocations located at the twin boundary and a Hirth dislocation lock having a Burgers vector of the $\frac{1}{6}\langle 002 \rangle$ type are also discussed.

§1. INTRODUCTION

High-resolution electron microscopy (HREM) has been extensively used to study the defect structures in various elemental semiconductor materials, such as Si and Ge (Spence, O'Keefe and Kolar 1977, Desseaux, Renault and Bourret 1977, Olsen and Spence 1981, Bourret, Desseaux and Renault 1982), and III-V and II-VI compound semiconductors, such as CdTe (Sinclair, Ponce, Yamashita, Smith, Camps, Freeman, Erasmus, Nixon, Smith and Catto 1982), ZnSe (Shiojiri, Kaito, Sekimoto and Nakamura 1982, Mizera, Sundberg and Werner 1984), CdS (Echigoya, Pirouz and Edington 1982). In these diamond- and zincblende-like structures, a variety of complicated defects have been proposed, such as twins, mixed and screw dislocations, stacking faults terminated by Shockley or Frank partial dislocations, etc.

The structure of dislocation cores is of importance to the physical properties of crystals and in ZnS crystals it becomes more complicated because of the existence of two different sets of $\{111\}$ glide planes, the so-called glide set and shuffle set (Hirth and Lothe 1968). Olsen and Spence (1981) studied this problem and solved it by computer simulations. Bourret *et al.* (1982) discussed the Lomer dislocation in Si and Ge in detail.

In the zincblende structure, polarity exists and may cause some other types of twins, as suggested by Aminoff and Broomé (1931). Of course, the 180° rotation twin is common in these crystals (Mizera *et al.* 1984), but some authors have declared that they have observed the inversion twin in ZnSe crystals (Shiojiri *et al.* 1982).

The stacking fault energy of a crystal is an important physical parameter influencing properties. The weak-beam imaging technique (Cockayne, Ray and Whelan 1969) has been successfully used to measure the stacking fault energies of these

semiconductors (Takeuchi, Suzuki, Maeda and Iwanaga 1984). No experimental result on ZnS has yet been published, although the above authors have given a rough estimate recently.

In this paper, the results of a systematic investigation on the defects in ZnS crystals are presented. The HREM images of 180° rotation twins taken under different imaging conditions are discussed in detail, both experimentally and theoretically. End-on 60° mixed and 0° screw dislocations, the former dissociated into a 30° and a 90° Shockley partial, and the latter into two 30° Shockley partials, were also studied. By measuring the width of extended dislocations from HREM micrographs, the stacking fault energy of ZnS on {111} planes has been determined by using anisotropic elasticity theory of dislocations to be $2.7 \pm 0.1 \text{ mJ m}^{-2}$. Finally, two kinds of Frank dislocation located at the twin boundary and a Hirth dislocation lock are discussed.

§2. EXPERIMENTAL

Specimens were vapour-grown crystals. They were ground in an agate mortar, the ground powders were immersed in methanol and then collected on a perforated carbon foil.

High-resolution electron microscopy observations were performed with a JEM-200CX electron microscope using the ultra-high-resolution pole-piece ($C_s = 1.2 \text{ mm}$ at 200 kV) with a $\pm 10^\circ$ double-tilting goniometer stage at an accelerating voltage of 200 kV. Images were obtained using nine beams (transmitted beam and eight diffracted beams) since the objective aperture was limited to 5.5 nm^{-1} . Typical illumination divergence is $1.5 \times 10^{-3} \text{ rad}$. The resolution limit δ_c given by the damping function is 0.2 nm (the main limitation of the resolution is caused by the thermal spread of the emitted electrons) and the Scherzer resolution is 0.26 nm, which is characterized by the contrast transfer function. In these conditions, close atom pairs projected on {110}, about 0.14 nm apart, are not resolved. A LaB_6 filament was fitted to the microscope used for this work and the image astigmatism was adjusted using the characteristic minimum contrast condition of the amorphous carbon film. Voltage centring was used to align the microscope, since the chromatic aberration from the energy spread of electrons leaving the filament was found to be more important than fluctuations in objective lens current.

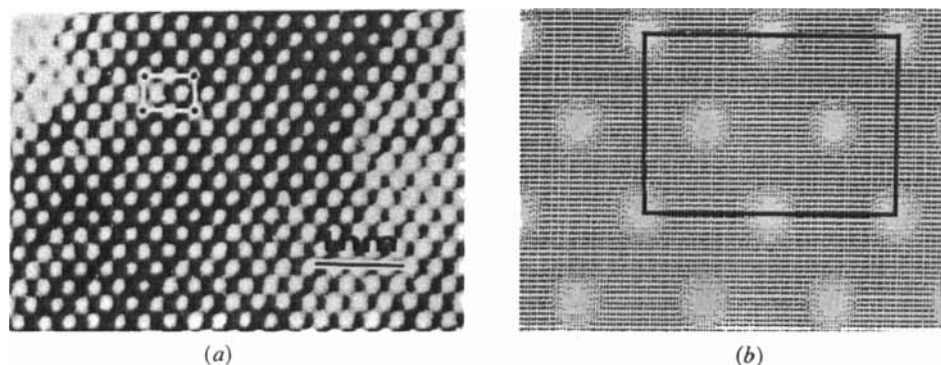
Image simulation was carried out using the multi-slice program written by Dr. K. Ishizuka, where a fast Fourier transformation (FFT) routine was introduced in calculating the convolution (Ishizuka and Uyeda 1977) in order to increase the speed of the computations. The slice thickness was taken to be 0.382 nm.

§3. IMAGE INTERPRETATION

The important parameters for interpretation of the contrast are the specimen thickness (t) and the defocusing distance (Δf). The specimen thickness is more difficult to determine and it demands a great deal of experience for each particular material. Using the dynamical *Pendellösung* fringes, thickness fringes along $\langle 110 \rangle$ rows are calculated. Amplitudes of the 000 and 111 beams oscillate with thickness with a characteristic length ξ_{000} or ξ_{111} (Spence *et al.* 1977, Spence, O'Keefe and Iijima 1978) and because HREM images are always taken near the specimen edge, the thickness may thus be estimated within $\pm \xi_{000}/4$.

It is our experience that observations have to be limited to the thickness range of $\xi_{000}/4$ to ξ_{000} where $\xi_{000} \approx 15 \text{ nm}$. For larger values the images are too sensitive to the exact orientation. The defocusing distance was estimated by a priori knowledge.

Fig. 1



(a) Characteristic HREM image of ZnS with 110 beam incidence and (b) computer-simulated image. Bright dots in the image correspond to either atomic column pairs ($\Delta f = -65$ nm) or structural channels ($\Delta f \approx -90$ nm). Unit cell is outlined, vertical bar = 0.542 nm.

Much the same as the elemental semiconductors, the HREM images of ZnS usually appear in the form shown in fig. 1 (a). However, the bright dots may either correspond to atomic column pairs or to structural channels surrounded by atoms, depending on the defocusing distance. Detailed computer simulation was in agreement with the result shown in fig. 1 (b). In general, we may deduce the following common rules within the thickness range of 4 to 15 nm:

- (a) $\Delta f \approx -65$ nm (Scherzer defocus), a bright dot corresponds to an atomic column pair;
- (b) $\Delta f \approx -95$ nm, a bright dot corresponds to a structural channel, i.e. contrast reversal occurs.

On the other hand, if planar defects exist, such as stacking faults and twin boundaries, characteristics of the bright dot may also be defined, according to Olsen and Spence (1981), by the symmetries of their HREM images (see figs. 4 and 5).

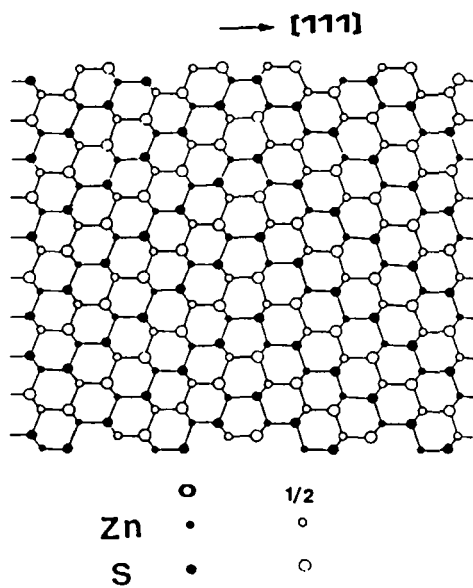
§ 4. RESULTS AND ANALYSIS

4.1. 180° rotation twins

In the zincblende structure, there may be several types of twins (Aminoff and Broomé 1931). However, 180° rotation twins are more common than others; the structure projected along a $\langle 110 \rangle$ direction is shown in fig. 2. The rotation axis is $\langle 111 \rangle$ and fig. 3 is a general view of the twin structure in ZnS, from which a high density of twins can be clearly seen.

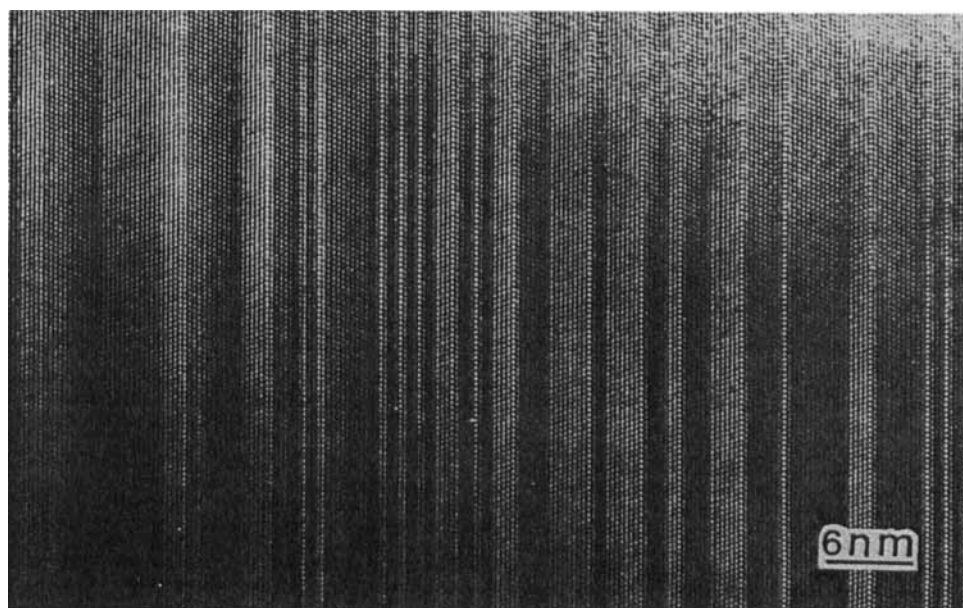
As pointed out in § 3, the bright dots in the HREM image observed may correspond to different structural elements (either atomic column pairs or structural channels) and we may thus predict that the twin boundary should appear in different forms if the experimental parameters are changed. The experimental and computer-simulated images are both shown in figs. 4 and 5. The bright dots represent atom pair columns and tunnels respectively. The simulated images were carried out by using the periodic continuity (Cowley 1975) and the superlattice was assumed to contain 48 atoms, six times that of the original cubic unit cell. The defocusing distance is about -65 and -90 nm, respectively, with a thickness of $t \approx 7$ nm for both cases.

Fig. 2



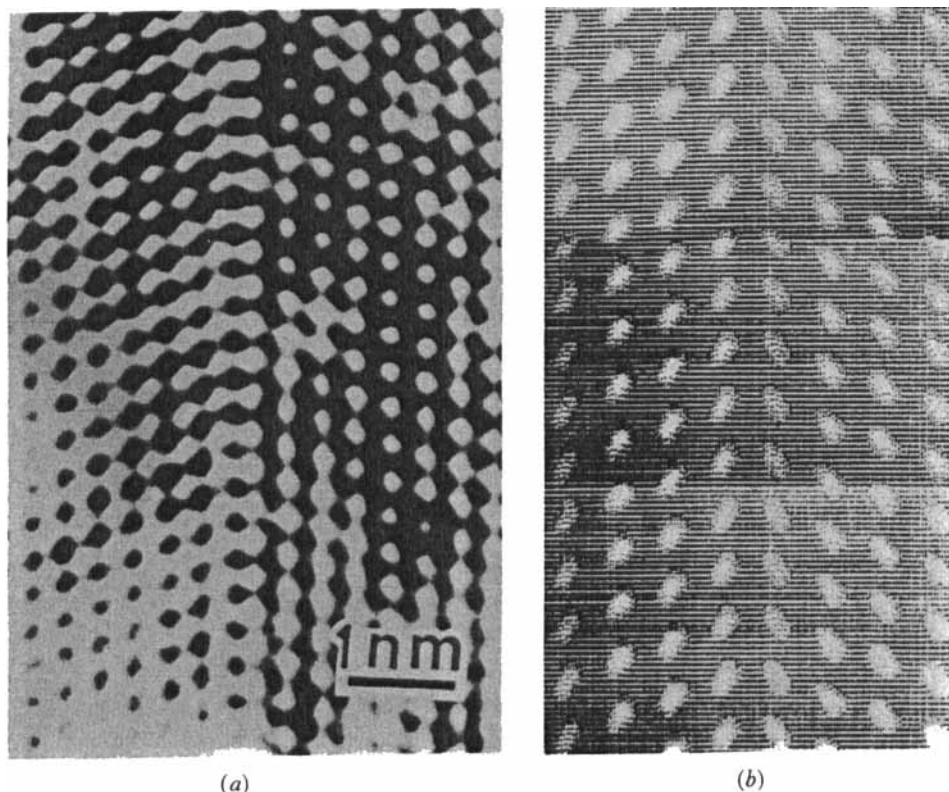
Structural model for 180° rotation twin. [111] is the rotation axis.

Fig. 3



A general view of the structural image showing a high density of twins in ZnS.

Fig. 4



(a) Structural image compared with (b) simulated image with $\Delta f \approx -65$ nm and $t \approx 7$ nm. A bright dot represents an atomic column pair (compare fig. 2).

4.2. End-on extended dislocations

In diamond- and zincblende-like crystals, a dislocation with Burgers vector of the $\frac{1}{2}\langle 110 \rangle$ type usually dissociates into two partials with a stacking fault between them forming an extended dislocation. If we assume the electron beam incident direction is along $[1\bar{1}0]$, the end-on dislocation with Burgers vector $\frac{1}{2}[10\bar{1}]$ will be a 60° mixed dislocation and an end-on screw dislocation will have a Burgers vector of $\frac{1}{2}[1\bar{1}0]$. The expression for the dissociation of a 60° dislocation will be

$$\frac{1}{2}[10\bar{1}] \rightarrow \frac{1}{6}[2\bar{1}\bar{1}] + \frac{1}{6}[11\bar{2}],$$

where $\frac{1}{6}[2\bar{1}\bar{1}]$ and $\frac{1}{6}[11\bar{2}]$ are the Burgers vector of a 30° Shockley partial and a 90° Shockley partial, respectively.

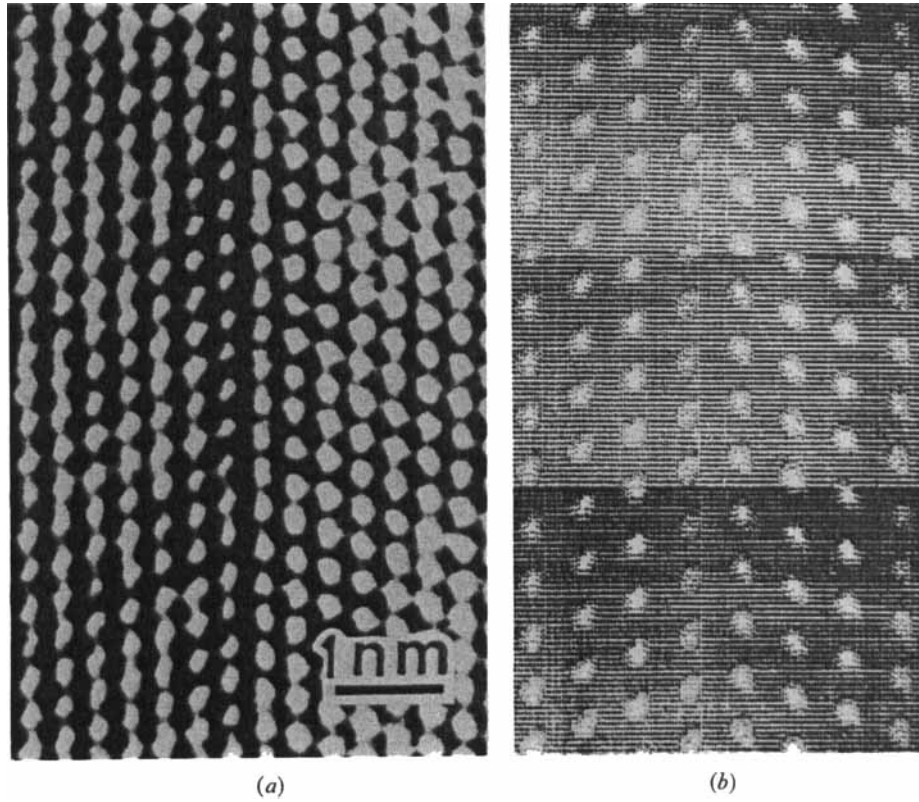
Making use of the Thompson tetrahedron notation, such a dissociation can also be expressed by:

$$BC \rightarrow B\delta + \delta C,$$

as indicated in fig. 6.

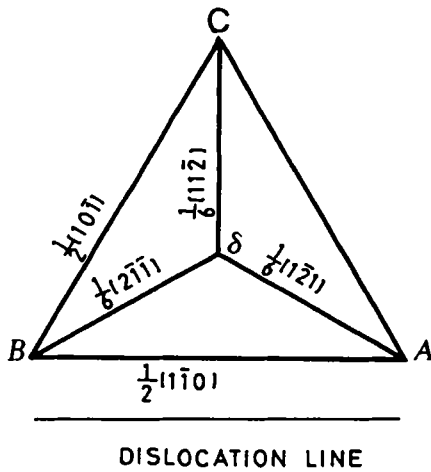
Figure 7 shows an observed micrograph of an end-on extended dislocation. If we draw a Burgers circuit around the whole extended dislocation, i.e. involving both partials, we can get the Burgers vector projected onto the $(1\bar{1}0)$ plane to be $\frac{1}{4}[11\bar{2}]$,

Fig. 5



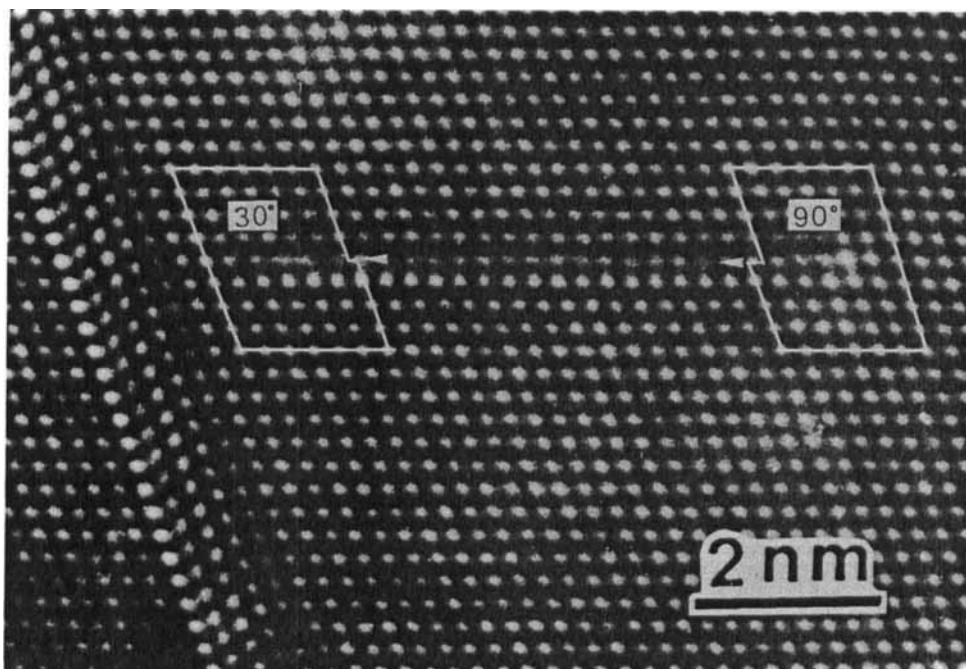
(a) Structural image and (b) simulated image of the 180° rotation twin with $\Delta f \approx -95$ nm and $t \approx 7$ nm. A bright dot represents a structural channel, i.e. image contrast reversed in comparison with fig. 4.

Fig. 6



Thompson tetrahedron projected along $D\delta$.

Fig. 7



Structural image of an end-on 60° dislocation dissociated into 30° and 90° partials, connected by a strip of intrinsic stacking fault. Only the edge components of the dislocation are indicated by the arrows in the Burgers circuits around the partials.

which is the projection of $\frac{1}{2}[10\bar{1}]$. Therefore, we may conclude that this extended dislocation was formed by a dissociation from a 60° dislocation. Similarly, if Burgers circuits of the two Shockley partials, starting and ending at the fault, were drawn as indicated in fig. 7, one can easily determine the 90° Shockley and 30° Shockley partials, respectively, by their projected vectors onto $(1\bar{1}0)$ plane, which are $\frac{1}{8}[11\bar{2}]$ and $\frac{1}{2}[11\bar{2}]$ respectively.

According to the micrograph, it can be determined that the stacking fault between the two partials is an intrinsic one and that the bright dots in the image correspond to the atomic column pairs, by using the rules proposed by Olsen and Spence (1981).

By utilizing the same analysing procedure mentioned above, it was found that the end-on extended dislocation shown in fig. 8 was formed by a 0° screw dislocation (its projection on $(1\bar{1}0)$ being of zero length), dissociated into two 30° Shockley partials by the expression

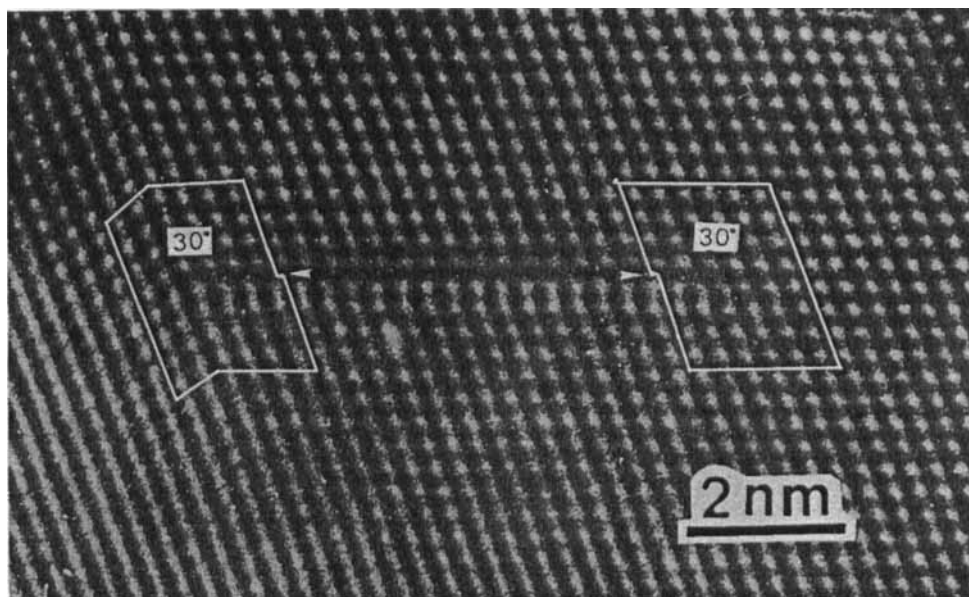
$$\frac{1}{2}[1\bar{1}0] \rightarrow \frac{1}{8}[2\bar{1}\bar{1}] + \frac{1}{8}[1\bar{2}1].$$

The corresponding Thompson notation is

$$BA \rightarrow B\delta + \delta A$$

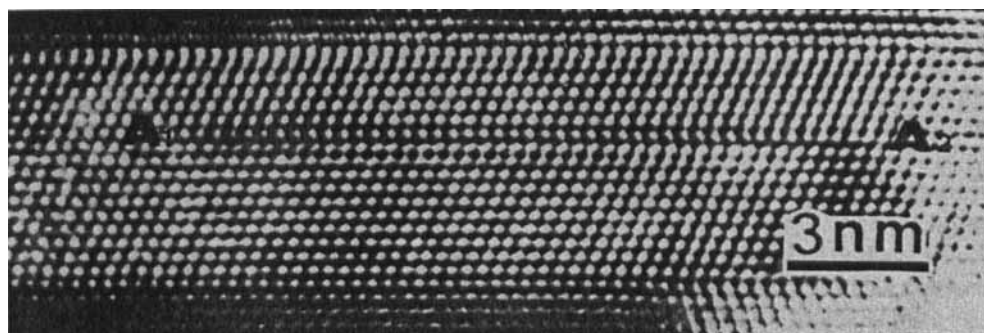
and the two Shockley partials are of the same magnitude but in opposite directions on the projection plane $(1\bar{1}0)$, as indicated by the arrows in fig. 8. The stacking fault between the partials is also an intrinsic one. One may see that in fig. 8 there is a microtwin at one end of this extended dislocation.

Fig. 8



Structural image of an end-on screw dislocation dissociated into two 30° partials, connected by a strip of intrinsic stacking fault. The edge components of these two partials, which have the same magnitude but opposite signs, are indicated by arrows.

Fig. 9



A dissociated 0° screw dislocation having a width of about 12.9 nm, corresponding to a stacking fault energy of 2.7 mJ m^{-2} .

4.3. Stacking fault energy

When a dislocation dissociates into two partials forming an extended dislocation, the width of it can be used to calculate the stacking fault energy by using the anisotropic elasticity theory of dislocations, if the elastic coefficients are known (Hirth and Lothe 1968). Using the elastic coefficients given by Zarembovitch (1963), the stacking fault energy on $\{111\}$ planes in ZnS crystals has been determined to be $2.7 \pm 0.1 \text{ mJ m}^{-2}$, which is in agreement with the value ($< 6 \text{ mJ m}^{-2}$) estimated by Takeuchi *et al.* (1984). The width of dissociation was defined by fig. 9, which is an HREM image of a 0° split end-on dislocation, to be about 12.9 nm.

4.4. Frank dislocations located at the twin boundary

Since a single atomic column cannot be resolved, for simplicity the notation for the stacking sequence

$$a\alpha b\beta c\gamma a\alpha b\beta c\gamma \dots$$

was reduced to the form

$$A B C A B C \dots,$$

where a, b, c and α , β , γ represent a Zn atom layer and a S atom layer, respectively. The 180° rotation twins thus can be expressed as

$$\dots A B C A B C B A C B A \dots,$$

↑

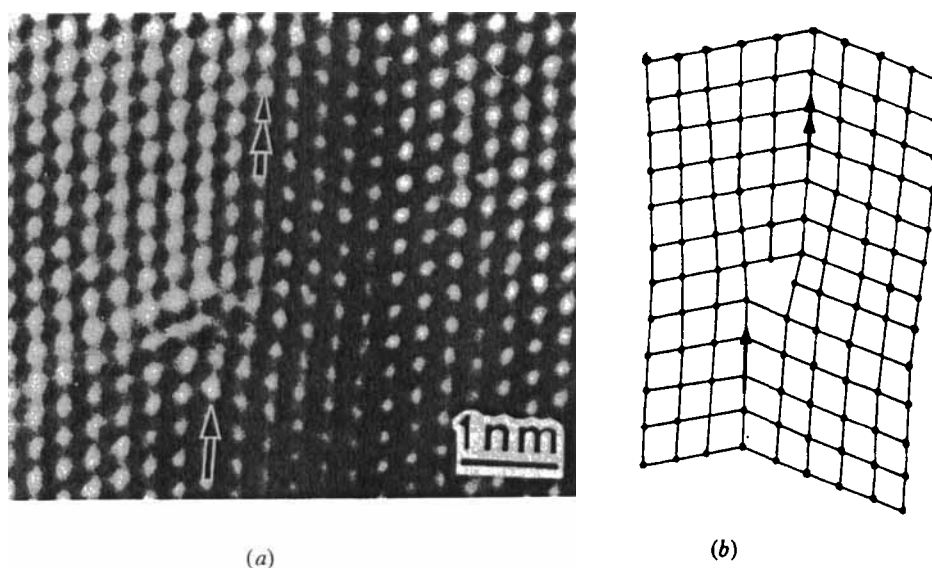
where the single arrow indicates the twin plane. In such a case, if an extrinsic Frank dislocation was introduced at the twin boundary, i.e. two extra atomic half-planes (one Zn layer and one S layer) inserted close to the twin plane, the stacking sequence would change to

$$\dots A B C A B A C B A C B A \dots,$$

↑ ↑

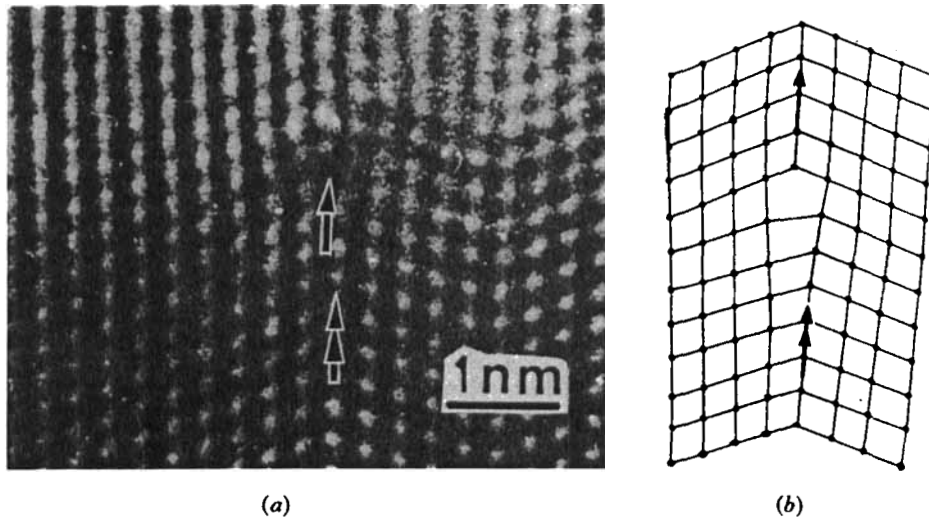
where the double arrows indicate the new twin plane after introducing an extrinsic Frank dislocation at the twin boundary, and the stacking unit A between these two arrows is the inserted half-planes. Therefore, the final result is that the twin plane is moved by two stacking units. Such a result has been confirmed by our experimental observations, as shown in fig. 10(a). Figure 10(b) is the corresponding structural model, a dark spot corresponding to a structural channel. In fig. 10 the original and new twin planes are marked respectively with single and double arrows.

Fig. 10



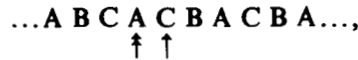
An extrinsic Frank dislocation located at the twin boundary which had caused the movement of the twin plane by two stacking units: (a) structural image; (b) structure model. Single and double arrows represent respectively the original and new twin planes.

Fig. 11



(a) Structural image and (b) structure model of an intrinsic Frank dislocation located at the twin boundary which had caused the movement of the twin plane (single arrow) by only one stacking unit to a new position (double arrows).

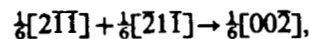
Similarly, if an intrinsic Frank dislocation was introduced at the twin boundary, the stacking sequence would be changed to



where the arrows have the same meaning as above. Both the experimental image and its corresponding structural model are given in fig. 11.

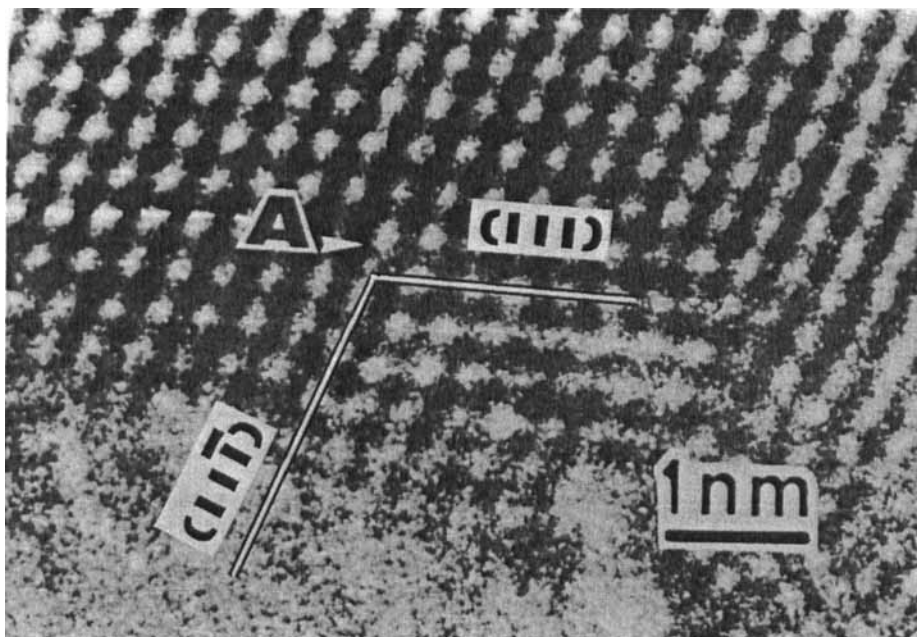
4.5. Hirth dislocation lock

In f.c.c. crystals, there are four equivalent $\{111\}$ glide planes. If two extended dislocations glide on two different $\{111\}$ planes and intersect, a so-called stair-rod dislocation may form, thus generating a dislocation lock. There are different types of dislocation lock, normally classified as a Lomer–Cottrell lock or a Hirth lock according to whether the Burgers vector belongs to the $\frac{1}{2}\langle 011 \rangle$ type or not. By examining the angle between these two $\{111\}$ glide planes, the two classes of dislocation may be distinguished (Friedel 1964): the acute angle corresponds to a Lomer–Cottrell lock and the obtuse angle to a Hirth lock. From the angle between the two extended dislocations, it can be determined that the dislocation lock in fig. 12 is a Hirth lock, which was thought to be a rarely observed type, with Burgers vector of $\frac{1}{2}\langle 002 \rangle$ type as the lowest energy state of this class. By detailed examinations, it can be concluded that the stair-rod dislocation (end-on) forming the lock was generated by reaction of two 30° Shockley partials:



and these two extended dislocations have Burgers vectors $\frac{1}{2}[10\bar{1}]$ and $\frac{1}{2}[\bar{1}10]$ lying on (111) and $(1\bar{1}\bar{1})$ respectively.

Fig. 12



A Hirth lock where the stair-rod dislocation has the Burgers vector of $\frac{1}{2}\langle 002 \rangle$ type. Such a lock was formed by the intersection of a 60° dissociated dislocation and a 0° dissociated dislocation which glide on different $\{111\}$ planes.

§ 5. DISCUSSION

5.1. Twin structures

Besides the 180° rotation twin, there are several other types of twin structures. One of them is the inversion twin investigated by Shiojiri *et al.* (1982) using HREM. However, these twin structures must have the stacking sequences of a type such as

$aaab$

which is a higher energy state because of destruction of bonds (Amelinckx 1979). On the other hand, our calculations have shown that all the images can be interpreted as a 180° rotation twin and the slight asymmetry of the twin boundary can be explained by the different scattering abilities of Zn and S.

In fact, owing to the presence of two different kinds of scattering elements, in the micrograph where a single atomic column was unresolved the bright dot corresponds neither to the geometrical centre of an atom pair nor to that of one structural channel.

5.2. Stacking fault energy determination

Although the weak-beam imaging technique has been successfully used to determine the stacking fault energy in crystals, HREM may have some advantages:

- (a) greater accuracy because the width of dissociation can be measured in the unit of lattice constants rather than by the magnetic magnification;
- (b) the stacking details can be given at the atomic level, and the dislocation cores may also be recognized at the same time if the instrument has a higher resolution, which might be reached in the near future.

Generally, an intrinsic stacking fault will have an energy twice as high as that of the intrinsic one and this may be the reason why an extrinsic fault rarely occurs.

5.3. Frank dislocations and the twin boundary

As shown in figs. 10 and 11, the Frank dislocations are located at the twin boundary and it causes a movement of the twin plane. It is evident that a single partial dislocation accompanying a stacking fault would generate a microtwin. For example, an intrinsic stacking fault introduced in the f.c.c. crystals (3C) will generate a new stacking sequence ABCBCABC... with a microtwin CBC in it. Naturally, a partial dislocation located at the twin boundary is a more probable state.

§6. CONCLUSIONS

Structures of twins and dislocations in ZnS have been studied by means of HREM. Structural images of 0° and 60° split dislocations and various Shockley and Frank partials, and also the Hirth dislocation lock have been obtained.

- (1) In cubic zinc sulphide crystals, there is a high density of 180° rotation twins. The twin boundary may appear differently in HREM micrographs; the asymmetry in the images is caused by the different scattering abilities of the two kinds of constituent atoms, or rather by the lack of a centre of symmetry in the space group.
- (2) The stacking fault energy of ZnS on {111} planes determined from the width of an extended dislocation is $2.7 \pm 0.1 \text{ mJ m}^{-2}$. Measuring the width of an end-on split dislocation by HREM has a higher accuracy which avoids the error in magnetic magnification.
- (3) A variety of dislocations exist in ZnS crystals, such as 30° and 90° Shockley partials, extrinsic and intrinsic Frank partials, 60° and 0° split dislocations and the Hirth lock with Burgers vector of $\frac{1}{2}\langle 002 \rangle$ type. Partial dislocations located at the twin boundary were found to be in a stable state.

ACKNOWLEDGMENTS

The authors wish to thank Drs X. Luo and W. N. Liu, Changchun Institute of Physics, Academia Sinica, for providing the ZnS crystals and Drs L. M. Clarebrough, A. Olsen and H. Q. Ye for useful discussions.

REFERENCES

- AMELINCKX, S., 1979, *Dislocations in Crystals* (Amsterdam: North-Holland).
 AMINOFF, G., and BROOMÉ, G., 1931, *Z. Kristallogr. Kristallgeom.*, **80**, 355.
 BOURRET, A., DESSEAUX, J., and RENAULT, A., 1982, *Phil. Mag. A.*, **45**, 1.
 COCKAYNE, D. J. H., HONS, A., and SPENCE, J. C. H., 1980, *Phil. Mag. A.*, **42**, 103.
 COCKAYNE, D. J. H., RAY, I. L. F., and WHELAN, M. J., 1969, *Phil. Mag.*, **20**, 1265.
 COWLEY, J. M., 1975, *Diffraction Physics* (Amsterdam: North-Holland).
 DESSEAUX, J., RENAULT, A., and BOURRET, A., 1977, *Phil. Mag.*, **35**, 357.
 ECHIGOYA, J., PIROUZ, P., and EDINGTON, J. W., 1982, *Phil. Mag. A.*, **45**, 455.
 FRIEDEL, J., 1964, *Dislocations* (Oxford: Pergamon Press).
 HIRTH, J. P., and LOTHE, J., 1968, *Theory of Dislocations* (New York: McGraw-Hill).
 ISHIZUKA, K., and UYEDA, N., 1977, *Acta crystallogr. A.*, **32**, 740.
 MIZERA, E., SUNDBERG, M., and WERNER, P., 1984, *Phys. Stat. Sol. (a)*, **85**, 83.
 OLSEN, A., and SPENCE, J. C. H., 1981, *Phil. Mag. A.*, **43**, 945.

- SHIOJIRI, M., KAITO, C., SEKEMOTO, S., and NAKAMURA, N., 1982, *Phil. Mag. A*, **46**, 495.
SINCLAIR, R., PONCE, F. A., YAMASHITA, T., SMITH, D. J., CAMPS, R. A., FREEMAN, L. A., ERASMUS, S. J., NIXON, W. C., SMITH, K. C. A., and CATTO, C. J. D., 1982, *Nature, Lond.*, **298**, 127.
SPENCE, J. C. H., O'KEEFE, M., and IJIMA, S., 1978, *Phil. Mag. A*, **38**, 463.
SPENCE, J. C. H., O'KEEFE, M., and KOLAR, H., 1977, *Optik*, **49**, 307.
TAKEUCHI, S., SUZUKI, K., MAEDA, K., and IWANAGA, H., 1984, *Phil. Mag. A*, **50**, 171.
ZAREMBOVITCH, A., 1963, *J. Phys., Paris*, **24**, 1097.